Rapid Communications

Resonantly enhanced inner-orbital ionization in molecular iodine

Dale L. Smith and George N. Gibson *
Department of Physics, University of Connecticut, Storrs, Connecticut 06269, USA

(Received 10 November 2017; published 8 February 2018)

We present a wavelength study of the strong-field single-electron ionization of molecular iodine near its one-photon B-state resonance at 530 nm. We have previously identified two ionization channels [Phys. Rev. A **95**, 013410 (2017)]: ionization of the high-lying molecular orbitals and ionization of the deep orbitals in I_2. We find a resonantenhancement of both channels, although the peakenhancement occurs at different wavelengths for the different channels.Moreover, the branching ratio of the ionization of the deep orbitals shows a dispersion-like function, with the branching ratio of the deep orbitals reaching over 98% at 519 nm. Finally, the branching ratio of double ionization into an excited state of I_2^{2+}as a function of wavelength closely matches the branching ratio of the single ionization of deep orbitals, implying that excitation of molecular ions generally comes about through inner orbital ionization. These findings are inconsistent with current molecular ionization theory.

DOI: 10.1103/PhysRevA.97.021401

Most strong-field interactions with atoms and molecules, such as high-harmonic-order generation (HHG), start with single-electron ionization [1]. In atoms and light molecules, most of the ionization comes from the least bound electron in either the outer shell for atoms or the highest-occupied molecular orbital (HOMO) for molecules [2]. The influence of inner orbitals can be seen in the strong-field molecular interaction, but the angularly averaged ionization rate from the inner orbitals is small (<10%) [3]. We have shown in previous experiments that this is not the case for iodine. In fact, the branching ratio for ionization of the inner orbitals can exceed90% [4].We have also recently observed an interesting wavelength dependence to the ionization rates of the different orbitals [5]. Both of these results run counter to a simple tunneling model of strong field ionization, in that tunneling ionization strongly prefers the least bound electron and predicts no wavelength dependence [6].

In this Rapid Communication, we present a detailed study of the single ionization of I_2 in the vicinity of the X to B state resonance in the neutral molecule, where we previously saw a large wavelength effect on ionization. Since the $X-B$ transition involves driving an electron from the HOMO to the lowest-unoccupied molecular orbital (LUMO), one might expect that ionizing I_2 at this resonance would simply enhance the ionization rate of theHOMO, as that electronwould be promoted to the LUMO, where it should easily ionize. However, it turns out the results are significantly more complicated and counterintuitive.We divide the ionization signal intotwo parts: one corresponding to ionization of the HOMO, the HOMO-1 and HOMO-2, leading to the population of the X, A, and B states of the molecular ion, respectively [7,8]. We refer to this part as outer-orbital ionization (OOI). The other part of the ionization signal corresponds to ionization of deeply bound inner orbitals, or inner-orbital ionization (IOI). Both signals show a strong resonant behavior around the X to B transition, but the peaks in the two signals as a function of wavelength are slightly different. As a result, the branching ratio into the IOI channel shows a dispersion-type profile with the peak of the branching ratio exceeding 98%. At this point, the resonant interaction does not increase the ionization rate of theHOMO, but rather enhances the ionization rate of the inner orbital electrons. We speculate that driving the neutral molecule on a one-photon resonance creates a strong dipole that couples to the inner orbitals, leading to their large ionization rates, compared to the outer orbitals.

We use a Spectra Physics Ti:sapphire laser (800 μJ, 40 fs, 800nm, 1kHz) and send 450μJ of thebeam to aTOPAS optical parametric amplifier (OPA). The OPA generates short pulses from 489 to 680 nm with a pulse duration of 45 fs. For this experiment,wewere unable to cover the ranges of 525–550 and 590–626 nm with sufficient energy for ionization. We use the same experimental configuration as described inRef. [5]. In addition, we have introduced a pickoff mirror and photodiode after theOPA's prismcompressor tomonitor thebeam energy.We use the signal from the photodiode, which is sent to a Stanford Research Systems Boxcar, to remove energy variations which are longer than 30ms.We hold the energy to 1 uJ,which leads to a $1/\lambda^2$scaling in the intensity and corresponds to an intensity of $5.13 \times 10^{12}$to 2.7×10^{13} W/cm^2 for489 to 680nm. The pulse duration out of theOPAwasmeasuredwith anachromatic self-diffraction scanning autocorrelator.Room-temperature (295K) I_2 gas is diffused into a high–vacuum chamber to achieve a pressure of 7×10^{-7}Torr with a background pressure of 7×10^{-9}Torr. To achieve velocity map imaging (VMI) of ion fragments we use a three-element ion lens in conjunction with a microchannel plate (MCP) and phosphor screen which is imaged by a charge-coupled device (CCD) camera at a rate of 20 frames/s[5,9]. TheMCP is gated to slice the data and produces a temporal width of 15 ns. The camera rate corresponds to the boxcar averaging of the energy signal as described above. A typical ion image is shown in Fig. 1 with the laser polarized along the z axis as it is for all images. Data are taken in ion-countingmodewhere a threshold is applied to eachcamera

* george.gibson@uconn.edu

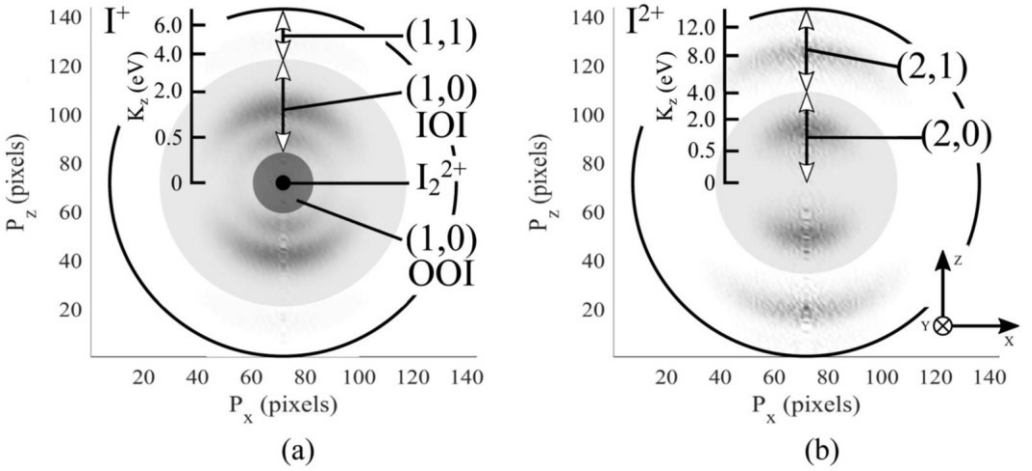

FIG. 1. Two deconvoluted VMI images which define the ionization channels. (a) The I^+ image has the I_2^{2+} at the center and is shown as a black circle. The OOI (1,0) channel is shown as a dark gray region outside of the I_2^{2+}. The IOI channel is shown as a light gray region and the remaining region to the outer black circle is the (1,1) channel. (b) The I_2^{2+} image shows the (2,0) channel as a light gray region. The rest of the image contained in the outer black circle shows the (2,1) which is not analyzed in this paper. The three axes are labeled in the image with the y axis being the time-of-flight axis. All data was taken with the laser polarization lying along the z axis.

pixel to determine if an ion was detected. This removes noise and fluctuations in the MCP response. For each wavelength, data were taken sequentially in the order I^+, I_2^+, and I_2^{2+} with 10 000 frames for I^+ and I_2^{2+} and 1000 frames for I_2^+.

Data were taken at 16 wavelengths around the neutral X to B state transition at 530nm [10]. The bounds of thewavelength range were set by the unusual enhancement in the IOI $I^{(1,0)}$ channel [throughout this paper (n,m) designates the $I_2^{(n+m)+} \rightarrow I^{n+} + I^{m+}$ dissociation channel]. This channel deviatesfrom its characteristic signal at 489 nm which sets the lower bound and returns to its normal pattern at the upper bound of 680 nm.

To analyze the VMI data, we begin by block averaging and folding the images in quadrature to improve statistics. Since we are interested in branching ratios, wemust havecompletely de-convolved images. However, the temporal detector gate leaves us with a thick slice and the resulting data cannot be deconvoluted with standard methods. To deconvolute the VMI data, we have modified the onion-peeling algorithm which allows us totransform partially slicedtwo-dimensional(2D) data [11,12]. However, this method requires knowledge of the slice thickness. Since the ion distribution has cylindrical symmetry, we can compare a slice at the center of the I^+ signal in the xz planetoasliceintheyzplane [13].Theyzslice is reconstructed from 29 slicedVMI images inwhich the gate delay is varied by 5 ns such that the entire I^+ signal is captured; see Fig. 2.Using this method, we find a 15-ns width for slicedVMI images. The modified onion-peeling algorithm allows us to back-project the higher energy contributions which occur in the thick sliced region to the lower energy pixels to invert the image. The images are then angularly integrated to restore the full information for each channel [14]. This allows us todetermine branching ratios for the various channels which we define below.

The I_2^+ signal corresponds to ionization of the HOMO and HOMO-1 resulting in the X and A states of the ion. However, some of the X- and A-state population can be excited to the dissociating B state. Direct ionization of the HOMO-2 can also populate the B state [5]. Thus, I^+ and low energy (1,0) constitutes the OOI signal. The B state dissociates with a KER of 0.025 to 0.21 eV. The IOI signalcomesfrom high KER (1,0) dissociation. We have previously shown that the high KER (1,0) signal cannot come from (1) direction ionization of an outer orbital, using energy conservation, as the energy levels at the equilibrium internuclear separation and the separated atom limit are known, and (2) a two-step process through the X or A states, using pump-probe and Fourier transform spectroscopy. For double ionization into the low-lying levels of the dication, we include I_2^{2+}, which has a known thermal width of 0.025 eV, and the (1,1) channel [5]. The (2,0) channel corresponds to electronically excited dications.

We measure the thermal width of the I_2^{2+} as described in Ref. [5] and find that it has a half-width half maximum of 0.019 eV. We therefore integrate the signal below 0.023 eV in

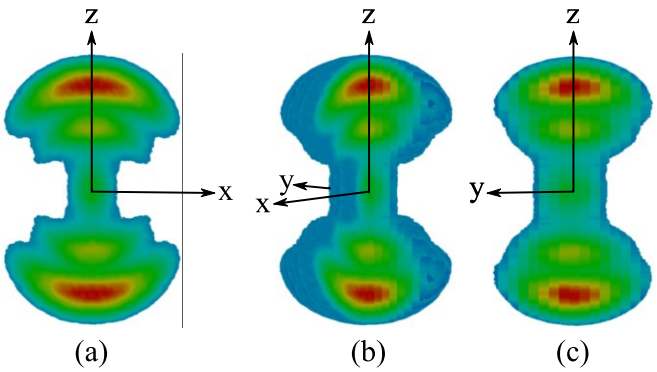

FIG. 2. 3D reconstruction of the $I^+(1,0)$ channels from sliced 490-nm VMI images [15]. The reconstructed image is composed of 29 slicedVMI images taken at consecutive gate delays which are 5 ns apart. Panel (a) shows the central slice VMI image in the xz plane, panel (b) shows the reconstructed three-dimensional (3D) image, and panel (c) shows the reconstructed slice in the yz plane. The central slice in the xz plane is compared to a central slice taken from the yz axis to determine the temporal width of the VMI gate.

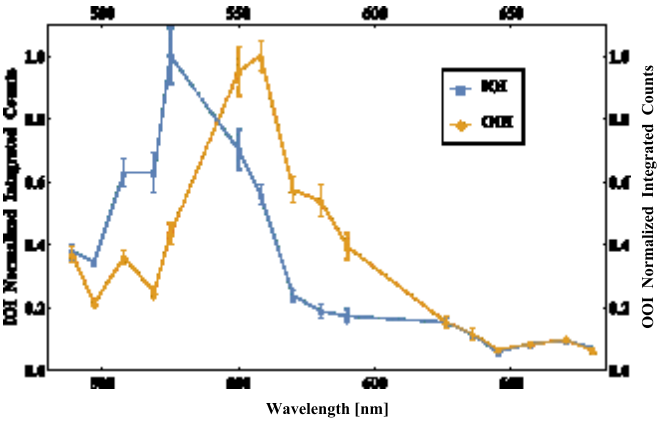

FIG. 3. The normalized integrated signals of the IOI and OOI as a function of wavelength. The peaks in the signals occur at different wavelengths. The dashed line show the region we are unable to cover. Error bars are calculated from uncertainty in the counting statistics and the pressure and intensity variation.

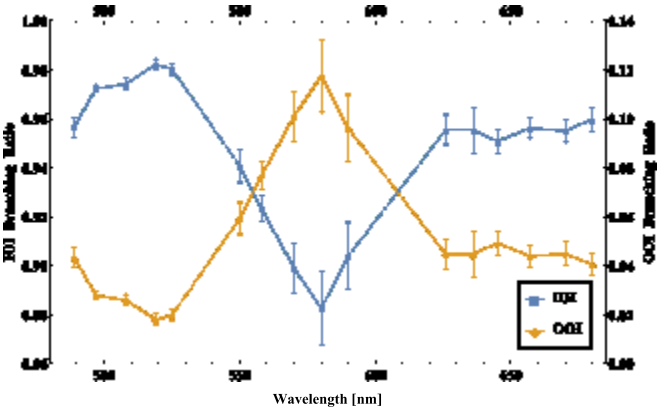

FIG. 4. Branching ratios of the IOI [IOI/(IOI + OOI)] and OOI [OOI/(IOI + OOI)] as a function of wavelength. The peaks in the ratios occur at different wavelengths and the IOI is strongly enhanced at 519 nm. The dashed line show the region we are unable to cover. Error bars are calculated from uncertainty in the counting statistics and the pressure and intensity variation.

the I_2^{2+} sum. For the (1,0) channel, we start with the B state, which has a known energy as described above. Therefore, for the OOI, we sum over all energies from 0.035 to 0.21 eV. We determine the region for the IOI channel from the images and sum the energies from 0.24 to 3.43 eV. All of the signal above 3.49 eV is taken in the (1,1) sum. In the I_2^{2+} images, the (2,0) and the (2,1) channels are well separated. We find that the (2,0) channel lies below 3.8 eV and the (2,1) is everything above 3.8 eV. This is shown in Fig. 1.

The uncertainty in the signals comes from three sources: (1) The uncertainties due to counting statistics are negligible. (2) Changes in the I_2 pressure during data taking aremonitored and contribute to the uncertainty. (3) Signals from images with intensities larger and smaller than the desired intensity range provide an upper bound to the uncertaintyfrom intensity fluctuations within the specified range.

In Fig. 3, we show the total integrated sum of the IOI and the OOI channels as a function of wavelength. At short wavelengths, between 489 and 508 nm, the two channels track well and at longer wavelengths, from 626 to 690 nm, the two channels have nearly the same wavelength dependence. However, in the region from 508 to 626 nm, we find that there is a difference in where the two channels peak, with the IOI peaking at a slightly shorter wavelength than the OOI. The branching ratios for these two channels, shown in Fig. 4, also show wavelength-dependent peaks for the two channels. The IOI channel has a branching ratio peak which coincides with the peak signal. Interestingly, the OOI branching ratio has a peak at 580 nm while the signal has a peak at 558 nm. Figure 5 shows that the VMI data clearly exhibits a dramatic change in the channel structure for this wavelength region, which only spans 200 nm. In particular, Figs. 5(b) and 5(c) differ in wavelength only by ~ 60 nm.

We also find that the double-ionization (2,0) channel has a wavelength dependence (Fig. 6). Interestingly, this dependence tracks well with the branching ratio of the IOI channel. There is an additional dip in the (2,0) channel which does not track with the IOI. This dip occurs at 508 nm and is on the same order as the dip in the branching ratio at 590 nm. This may be indicative of some other resonance effect.

Iodine has 106 electrons with the following molecular orbital (MO) structure [16],

$$(\text{core})^{92}\underbrace{(10\sigma_g)^2(10\sigma_u)^2}_{\text{inner valence}}\underbrace{(11\sigma_g)^2(6\pi_u)^4(6\pi_g)^4(11\sigma_u)^0}_{\text{outer valence}}. \quad (1)$$

IOI OOI

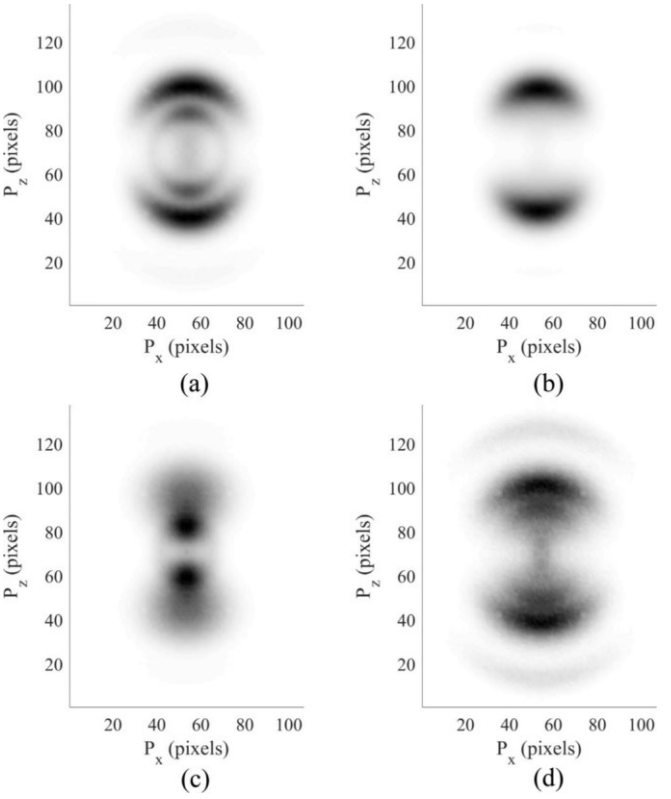

FIG. 5. Four I^+ VMI images corresponding to (a) the beginning of the data set at 489 nm, (b) the peak in the IOI branching ratio at 519nm, (c) the peak in the OOI branching ratio at 580nm, and (d) the end of the data set at 670 nm.

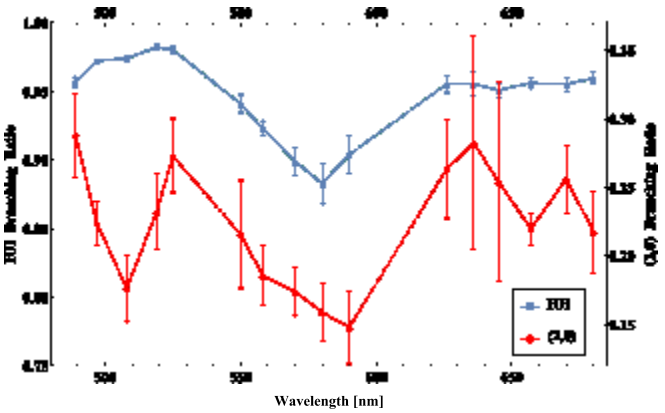

FIG. 6. Branching ratios of the OOI [OOI/(IOI + OOI)] and the (2,0) channel $[(2,0)/((2,0)+(1,1)+I_2^{2+})]$ as a function of wavelength. The two ratios track well above 519 nm. There is an unexplained dip in the (2,0) channel at 508 nm. The dashed line show the region we are unable to cover. Error bars are calculated from uncertainty in the counting statistics and the pressure and intensity variation.

Our previouswork shows that the IOI electrons play a role in ionization of iodine which is contrary to strong field ionization theory [5]. In this work, we have found that there is also a strong wavelength dependence to this ionization. As shown in Figs. 3 and 4, the ionization depends on the MO from which the electron is removed. Also, we see that there is a strong preference for the IOI as there is a 98% branching ratio at the peak at 519 nm. Such a strong wavelength dependence is likely to play a key role in higher order processes such as HHG. Since tunneling ionization theory does not directly predict inner orbital ionization the data suggestion the presence of an additional interaction. Reference [5] suggests that static (induced or permanent) dipoles influence the tunneling rate of different orbitals. In our experiment, we strongly drive a one-photon resonant dipole between the X and B states in the neutral molecule. This additional field appears to have a profound influence on the ionization rates of the inner orbitals. This effect can either enhance or suppress the IOI branching ratio, depending sensitively on the exact driving frequency.

For double ionization, we also see the influence of the IOI channels. Figure 6 shows that there is a similar wavelength dependence to the branching ratios of the IOI and the (2,0) channels. This implies that double ionization takes place through the IOI and leaves the double cation in an excited state.

Finally, these result may be connected to prior work in which the branching ratio of the (1,0) was seen to rise to nearly95% as a function of internuclear separation (R)[4]. The $X-B$ transition in neutral iodine shifts to lower frequency as R increases, bringing it into resonance with the 800-nm beam used in Ref. [4] at a distance of 5.71 a.u. The peak was seen in the data at a value of $R = 6.85$ a.u., where the $X-B$ transition is longer than 800 nm. However, the vibrational wave packet is moving in this experiment, affecting the phase.

Moreover, the phenomenon of enhanced ionization starts to play a role at large R [17].Nevertheless, it isremarkable that in these rather different experiments (thewavelength dependence at fixed R and the R dependence at fixed wavelength) both show an enhanced branching ratio for IOI, indicating that the strength of IOI depends on many factors and can dominate the ionization.

In conclusion, we find that there is an unexpectedly strong wavelength dependence in a narrow 200-nm region for the strong-field single-electron ionization of molecular iodine. This wavelength dependence does not occur at the same wavelength for the two single-ionization (IOI and OOI) channels. We speculate that the resonantenhancement of the IOI channel is brought about through a couplingbetweenmolecular orbitals brought on by a strong dipole. The double-ionization (2,0) channel has a wavelength dependence which correlates well with the single-ionization IOI channel, which suggests that double ionization takes place through excited states and deeply bound molecular orbitals.

We would like to acknowledge our support from the NSF under Grant No. NSF-PHYS-1707542.

[1] P. B. Corkum, Phys. Rev. Lett. **71**, 1994 (1993).
[2] B. K. McFarland, J. P. Farrell, P. H. Bucksbaum, and M. Gühr, Science **322**, 1232 (2008).
[3] H. Akagi, T. Otobe, A. Staudte, A. Shiner, F. Turner, R. Dörner, D.M. Villeneuve, and P. B. Corkum, Science **325**, 1364 (2009).
[4] H. Chen,V. Tagliamonti, andG.N.Gibson,Phys.Rev.Lett.**109**, 193002 (2012).
[5] D. L. Smith, V. Tagliamonti, J. Dragan, and G. N. Gibson, Phys. Rev. A **95**, 013410 (2017).
[6] M.V. Ammosov, N. B.Delone, and V. Krainov, Sov. Phys. JETP **64**, 1191 (1986).
[7] M. C. R. Cockett, R. J. Donovan, and K. P. Lawley, J. Chem. Phys. **105**, 3347 (1996).
[8] D. C. Frost and C. A. McDowell, Can. J. Chem. **38**, 407 (1960).
[9]A.T.J.B.EppinkandD.H.Parker,Rev. Sci. Instrum. **68**, 3477 (1997).
[10] J. Tellinghuisen, J. Chem. Phys. **76**, 4736 (1982).
[11] C. Bordas, F. Paulig, H. Helm, and D. L. Huestis, Rev. Sci. Instrum. **67**, 2257 (1996).
[12] J.Winterhalter,D.Maier, J.Honerkamp,V. Schyja, andH.Helm, J. Chem. Phys. **110**, 11187 (1999).
[13] R. Zare, Mol. Photochem. **4**, 1 (1972).
[14] B. Whitaker, *Imaging in Molecular Dynamics: Technology and Applications: A User's Guide* (Cambridge University Press, Cambridge, UK, 2003), pp. 227–245.
[15] H. Childs, E. Brugger, B. Whitlock, J. Meredith, S. Ahern, D. Pugmire, K. Biagas, M. Miller, C. Harrison, G. H. Weber *et al.*, in *High Performance Visualization: Enabling Extreme-Scale Scientific Insight* (CRC Press, Boca Raton, FL, 2012), pp. 357–372.
[16] J. S. Zhu, J. K. Deng, and C. G. Ning, Phys.Rev.A**85**, 052714 (2012).
[17] H. Chen, V. Tagliamonti, and G. N. Gibson, Phys. Rev. A **86**, 051403 (2012).